IEEE Open Journal of Antennas and Propagation

Received 1 January, 2024; revised 23 January, 2024; accepted 11 February, 2024. Date of publication XX Month XXXX; date of current version XX Month XXXX.

Digital Object Identifier **********

Simple and Low-Cost Shared-Aperture Antenna Module for 5G N78 and N257 Applications

Danle Ma, Jiawei Zhu, Runjie Diao, Ruiping Liang, Huiming Li, Jun Huang, Hui Tang (Member, IEEE), Yue Cao (Member, IEEE), and Jian-Xin Chen (Senior Member, IEEE)

School of Information Science and Technology, Nantong University, Nan Tong 226019, China.

CORRESPONDING AUTHOR: Hui Tang (e-mail: huitang16@hotmail.com).

This work was supported in part by the National Natural Science Foundation of China under Grant 62271271, in part by the Postgraduate Research and Practice Innovation Program of Jiangsu Province under Grant SJCX23_1783 and KYCX22_3344, in part by the Natural Science Foundation of Jiangsu Province under Grant BK20220602 and in part by the Nantong Basic Science Research Program under Grant JC12022065.

ABSTRACT A simple and low-cost shared aperture antenna module for 5G N78 and N257 applications is proposed. This module integrates a microwave (MW) patch antenna and a millimeter wave (MMW) substrate-integrated waveguide (SIW) slot antenna. The MW part employs splits etched on the patch and shorting vias to excite TM_{01}, TM_{20}, and TM_{21} modes simultaneously and generate a wide band covering N78 band. In the MMW part, beveled SIW cavities with additional metal vias are set on the same substrate of the patch antenna and extend the bandwidth of the slot antennas covering N257 band. The shared-aperture antenna module provides high port isolations, and high and flat gains for both bands. Moreover, the MMW beam scanning is manipulated in the E- and H-plane. A prototype is designed, implemented and measured for verification.

INDEX TERMS Microstrip patch antenna (MPA), microwave (MW) antenna, millimeter wave (MMW) antenna, shared-aperture, slot antenna.

I.INTRODUCTION

The fifth generation of communications (5G) necessitates the utilization of new frequency bands, encompassing sub-6 GHz microwave (MW) and millimeter-wave (MMW) bands [1], [2], to accommodate higher data rates and increasing capacity. The deployment of these new frequency bands undoubtedly amplifies the complexity in designing terminal antennas [3], [4]. Terminal devices require compact, low-cost antennas that can efficiently utilize space while supporting both MW and MMW channels. MW/MMW shared aperture antennas are considered a viable approach to address this challenge [5], [6]. When designing MW/MMW shared aperture antennas, it is typically necessary to ensure wide bandwidth coverage, high gain, and broad-angle coverage [7]. This is particularly crucial in the case of MMW frequencies, which suffer from significant transmission losses and weak diffraction capabilities, thereby imposing severe limitations on transmission distance and signal coverage [8]. Consequently, 5G MMW antennas should exhibit high-gain characteristics, typically exceeding 10 dBi, along with beam-steering capabilities [9].

To date, many large frequency ratio shared aperture antennas have been developed in several methods for effectively integrating low and high frequency radiation parts. The first method designs the low and high frequency radiation parts independently [10] - [14], The S-band metasurface antenna element is placed above the K-band gap array in [13], where the former element is invisible to the latter. It is proposed in [14] that a 2×2 28 GHz patch array nested in a 3.5 GHz circular patch antenna in a coplanar and shared adaptation manner achieves a broadband and high gain in the MMW band. However, the increased profile height and manufacturing costs of the antennas are unavoidably incurred by these designs due to their design complexity, regardless of their effectiveness at both high and low frequencies. Furthermore, restrictions on cell pitch settings are imposed, and independent performance control is complicated, with the typical isolation below 25 dB between the ports.

Compared to the above method, the second method achieves the advantage of high-density layout by embedding high- and low-frequency antennas into each other's structures offering the shared-aperture antennas [15], [16], [17]. In [18], a proposal is made for a dual-band microstrip grid array antenna that spans the 3.7 GHz and 28.5 GHz frequency bands. This antenna operates in grid array mode at high frequencies and switches to a patch antenna or mesh patch antenna mode at low frequencies. The utilization of shared-aperture antennas is enhanced, allowing for independent adjustments of operating frequencies and polarization modes. However,

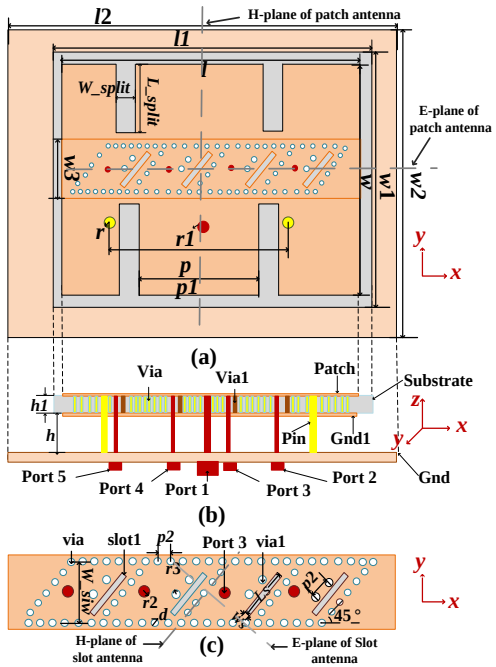

FIGURE 1 **Geometry of the proposed antenna. (a) Top view. (b) Side view. (c) Layout of slot array.**

***l* = 50 mm, *w* = 38 mm, *w1* = 70 mm, *l2* = 100 mm, *w2* = 100 mm, *w3* =8 mm, *L_split* = 13.5 mm, *W_split* = 2.5 mm, *r* = 0.5 mm, *P* = 37 mm, *P1* = 25 mm, *P2* = 1 mm, *d* = 0.4 mm, *W_siw* = 6 mm, *Ls* = 6.4 mm, *r2* = 0.3 mm, *p3* = 1.4 mm, *Ws* = 0.4 mm.**

challenges are faced by existing multiplexed shared-aperture antennas in concurrently meeting the high gain and broadband requirements of both frequency bands while maintaining a simple structure.

At the same time, 45° tilted polarization has recently gained attraction because the signal of interest always appears with an uncertain polarization in wireless communication applications [19]. This polarization is sometimes more important than traditional horizontal or vertical polarization, but the existing shared aperture antenna designs rarely mention 45° tilted polarization.

In this paper, a large-frequency ratio share-aperture antenna based on partial structural reuse is proposed for N78 and N257 applications, which combines a MW patch antenna with a MMW substrate-integrated waveguide (SIW) slot array, and achieves inherent high isolation between low- and high-frequency channels. Maintaining a low-cost and simple structure, both of the low- and high-frequency parts obtain the high gain and broadband performance. Each MMW radiation unit has a separate feed network, making it possible to synthesize beams manipulated in the E- and H-plane. A prototype is designed, manufactured and measured. Reasonable agreement is observed between the measured and simulated results.

II. ANTENNA CONFIGURATION AND DESIGN

In this section, the operation principle of the proposed antenna is investigated. Fig. 1 shows the configuration of the

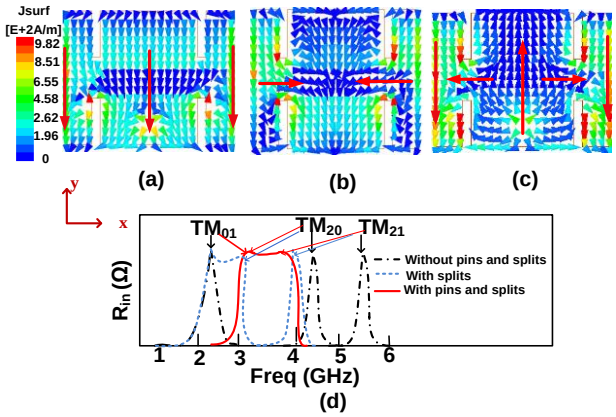

FIGURE 2 **Current distributions and input impedance of patch antenna. (a) TM_{01} mode. (b) TM_{20} mode. (c) TM_{21} mode. (d) Input impedance.**

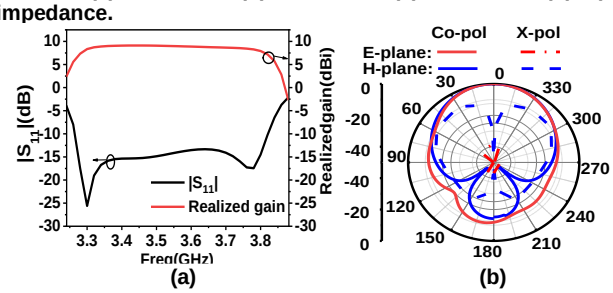

FIGURE 3 **Simulated results of patch antenna. (a) Reflection coefficient and gain. (b) Radiation patterns at 3.5 GHz.**

antenna. It consists of a rectangular patch with a size of (l×w) on a substrate ($l1$×$w1$) and a ground ($l2$×$w2$) with a distance of h = 4 mm below. The patch is constructed by Rogers 4003C with a dielectric constant of ε_{r1} = 3.55, a loss tangent of 0.0027, and a thickness of $h1$ = 0.508 mm. There are four splits with a spacing of $p1$ etched on the patch and a pair of shorting through holes with radius of r and a spacing of p are set on both sides of the feed. The MMW slot antenna array based on a SIW structure is embedded into the patch antenna on the same substrate, as shown in Fig. 1(c). The models are simulated and analyzed using ANSYA HFSS.

A. MW ANTENNA PART

As known, both odd- and even-order modes can be excited in a rectangular microstrip patch antenna (MPA) based on the cavity model for broadband radiation [20]. In this design, the TM_{01}, TM_{20}, and TM_{21} modes of the MPA are excited, and their current field distributions are shown in Fig. 2(a), (b) and (c), respectively. The input impedance curves in Fig. 2(d) show the changing of the resonant frequencies of the modes before and after splitting and shorting the patch. The two parallel splits decrease the resonant frequencies of the TM_{20} and TM_{21} modes, but have little effect on the TM_{01} mode. The resonant frequency of TM_{21} mode is reduced from 5.5 GHz to 3.8 GHz, and that of TM_{20} mode from 4.6 to 3.04 GHz. TM_{01} mode still resonates at the unchanged frequency. However, the middle part of the rectangular MPA is used to design MMW antennas, and the length of the two parallel splits is limited. A pair of short-circuit pins are then employed to increase the resonant frequency of the TM_{01} mode, but showing little influence on the TM_{20} and TM_{21}

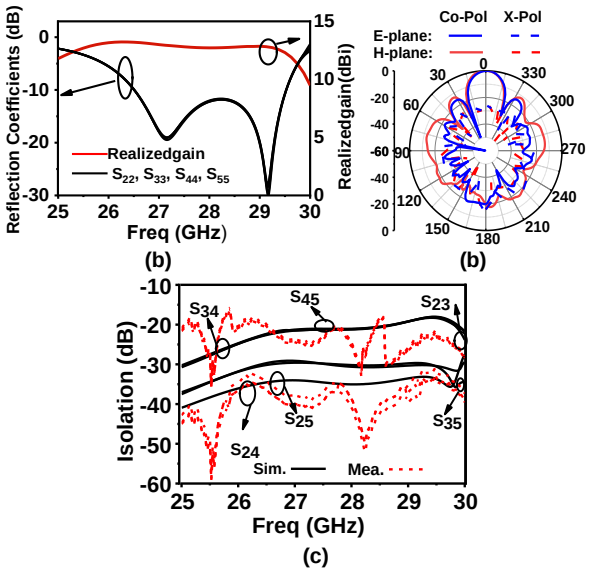

FIGURE 4. Simulated and measured results of slot array antenna. (a) Reflection coefficients. (b) Radiation patterns at 28 GHz. (c) Isolation between MMW elements.

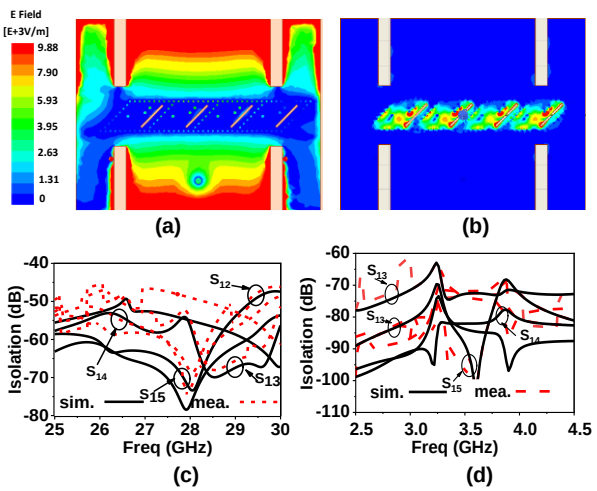

FIGURE 5 E-field distribution of the antenna (a) @ 3.5 GHz and (b) @ 28 GHz. Simulated and measured channel isolation in (c) MW band and (d) MMW band.

modes. With the pins at appropriate positions, the TM_{01} mode exhibits a resonant frequency of 3.26 GHz. The three modes resonate near enough to ultimately form a wide band for the MPA.

The simulation results of the designed MPA are shown in Fig. 3, including the reflection coefficient, the realized gain curves and radiation patterns. The impedance bandwidth of $|S_{11}|$ < -10 dB reaches 15.2% at the center frequency of 3.5 GHz. The in-band gain curve is flat, varying from 8.8 to 9.1 dBi. The radiation patterns are stable within the entire passband, with cross-polarization of the E- and H-plane less than -15 dB, as shown in Fig. 3(b).

B.MMW SLOT ANTENNA PART

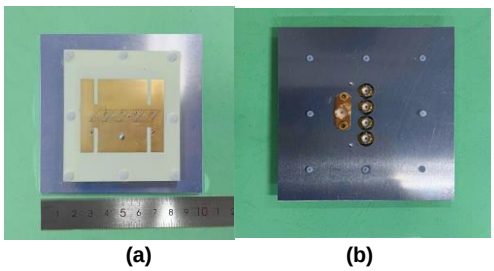

FIGURE 6 Photographs of the prototype. (a) Top view. (b) Bottom view.

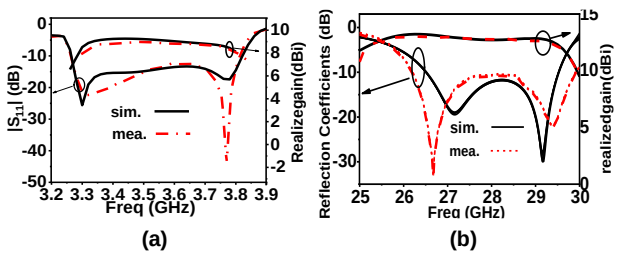

FIGURE 7 Simulated and measured S-parameters and boresight gains of the shared-aperture prototype. (a) MW part. (b) MMW part.

In each cavity, there is a slot etched parallel to the hypotenuse of the SIW, and a pair of metallic through-holes are located nearby the slot to achieve impedance matching. The arrangement of these two metallic through-holes aligns with the orientation of the slot. The introduction of metallic through-holes also induces a resonance for the slot antenna, consequently expanding its operational bandwidth. The separation between the slots and the slanted SIW metal through-holes is set at a distance of $\lambda_{hg}/4$. λ_{hg} is the guided wavelength at the center frequency of the desired MMW band. λ is the free-space wavelength at 28 GHz. The technical formula of the λ_{hg} is as follows,

$$\lambda_{hg} = \frac{\lambda}{\sqrt{1-\lambda^2/(2W_3)^2}} \quad (1)$$

$$W_{hsiw} = W_3/\sin 45^\circ \quad (2)$$

Fig. 4(a) predicts the simulated coefficient and gain results of the slot antenna array, which indicate that the simulated impedance bandwidth of $|S_{22}|$ < -10 dB reaches 11.1% at the central frequency of 28 GHz. The in-band gain curve exhibits a flat response, ranging from 11.7 to 12.1 dBi. Fig. 4(b) shows the simulated radiation patterns at the center frequency. Meanwhile, the slotted array elements are fed by coaxial lines, which help bind the feeding signal and weaken port correlation, resulting in an isolation of over 15 dB between individual MMW elements, as shown in Fig. 4(c).

C. CHANNEL ISOLATION

To achieve the high aperture utilization rate, a combination of the MPA and the slotted SIW array antenna is carried out to form a MW/MMW shared aperture antenna, as shown in Fig. 1. The MPA exhibits broadside radiation realized by stronger fields at its edges and weaker ones at the center part. The MMW slotted SIW array antenna is embedded into the same substrate at the center area of the MPA where weaker MW

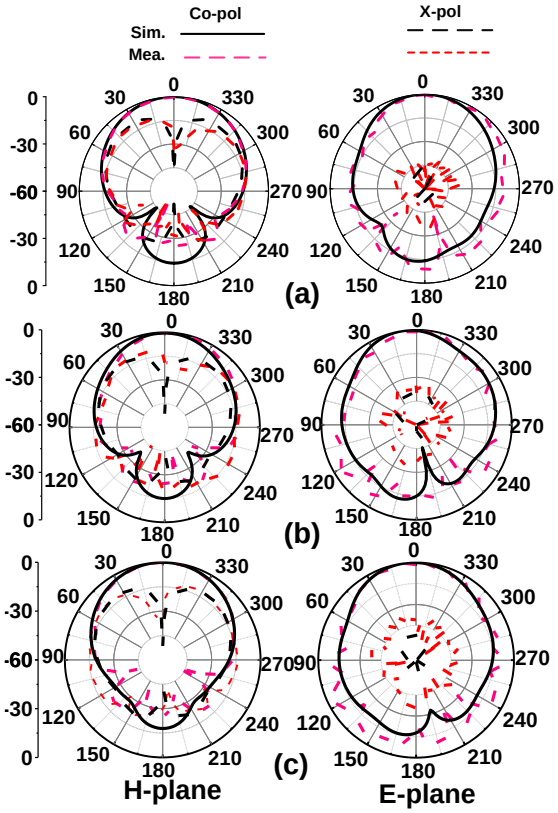

FIGURE 8 **The simulated and measured radiation patterns of the proposed MW antenna. (a) @ 3.28 GHz. (b) @ 3.5 GHz. (c) @ 3.78 GHz.**

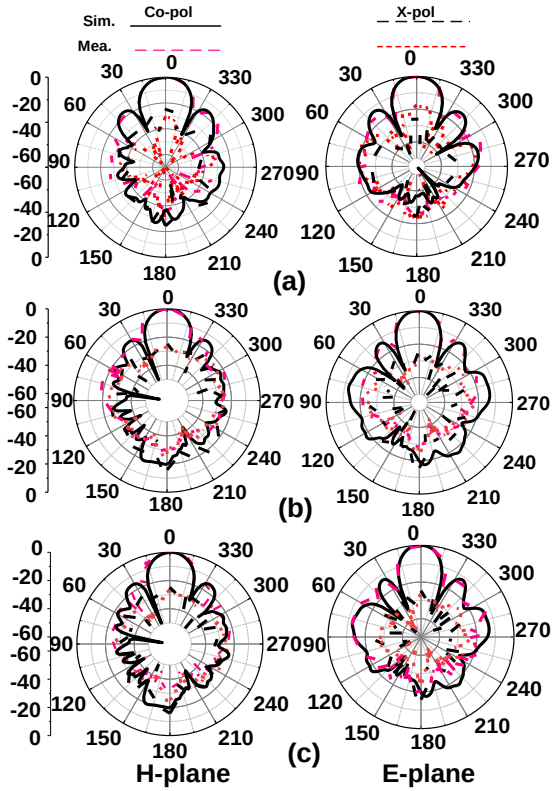

FIGURE 9 **The simulated and measured radiation patterns of the proposed MMW array antenna with equal-amplitude and in-phase feedings. (a) @ 26.5 GHz. (b) @ 28 GHz. (c) @ 29.5 GHz.**

fields locate, without little effect on the radiation of the MPA. Due to the good binding ability to the electromagnetic fields and inherent high-pass characteristics of SIW structures, the fields of MMW slot antenna and the MPA portion hardly leak into each other. The arrangement and these features of the shared aperture antenna effectively suppressing interference between the MW and MMW antennas and ensure a high level of channel isolation.

As shown in Fig. 5(a) and (b), it is seen that when the antenna works at 3.5 GHz, the electric fields are mainly concentrated on the microwave antenna part, and when it operates at 28 GHz, the electric fields focus on the area of the slot antenna. This demonstrates a high degree of isolation between the different parts on both frequency bands. Fig. 5(c) and (d) shows that the simulated isolations between the MW and MMW antennas exceed 65 dB when the MW MPA is active, and are larger than 45 dB when the MMW slot array antenna is in operation.

III. Implement and Results

In order to verify the design concept, a prototype of the proposed antenna is designed, fabricated and tested. Fig. 6 shows the photo of the realized Shared-aperture antenna.

Fig. 7 shows the simulated and measured reflected coefficients and realized gains. In the range of MW frequency, the measured -10 dB impedance bandwidth reaches 15.2%, ranging from 3.28 to 3.83 GHz which agrees with the simulated results and covers 5G N78 band, as shown in Fig. 7(a). Within the MMW frequency range, the tested 10-dB impedance bandwidth is 13.2%, spanning from 26.1 to 29.9 GHz and covering 5G N257 band, slightly outperforming the simulated one of 11.2%. The measured in-band gains exhibit relatively flat responses, with a peak of approximately 8.8 dBi for low frequencies and around 11.9 dBi for high frequencies. The measured performance deviates slightly from the simulation due to interface losses introduced by the subminiature version A (SMA) connectors and feeding cables used in the test, as well as minor processing errors.

Fig. 8(a), (b) and (c) show the measured and simulated patterns of the MPA on the E- and H- planes at 3.28, 3.5, and 3.78 GHz. Fig. 9(a), (b) and (c) present the radiation patterns of 45° tilted polarized MMW antenna at 26.5, 28, and 29.5 GHz. The measured results are in good agreement with the simulated ones. The in-band cross-polarization suppressions within the 3-dB beam are greater than 15 dB for the MW band and 25 dB for MMW band.

Fig. 10 shows the simulated and measured beam sweeping results of the MMW array antenna. Equation (3) is used to calculate the scanning performance of the array based on the measured active element pattern (AEP). When one component is tested, the other components are terminated with a 50 Ω load match [21].

TABLE 1 Performance Comparison with Existing Shared-Aperture Antennas

Ref	Center Frequency (GHz)	Impedance BW (%)	Peak Gain (dBi)	Electrical Dimension (λ_0^3)	Port isolation (dB)	Number of antenna elements	Antenna Type
[15]	3.5/60	5.3/6.4	7.3/11.5	0.42×0.3×0.03	100/60	1×12	Patch/Slot
[16]	5.8/29.2	3.5/4.6	10.9/18.7	0.42×0.36×0.04	38/32	4×16	Ground-surround patch/Slot
[17]	2.6/25	7/7.6	8/16	0.41×0.41×0.1	25	1×16	FSS/Slot
This work	**3.5/28**	**15.2/11.1**	**9.1/12.2**	**0.43×0.32×0.05**	**60/45**	**1×4**	**Patch/Slot**

λ_0 means the free-space wavelength at the center band of the microwave band.

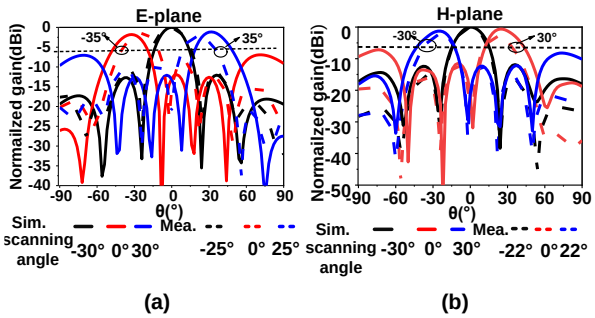

FIGURE 10 Simulation and measured results of beam scanning for MMW band. (a) E-plane. (b) H-plane.

$$E_{array} = \sum_{n=1}^{8} W_n E_n(\theta,\varphi) \exp[j(k\hat{r}\cdot r_n - \phi_n)] \qquad (3)$$

where $E_n(\theta,\varphi)$ is the measured AEP of the *n*th element, θ is the angle in the *xoz*-plane, and φ is the angle in the *xoy*-plane. W_n and ϕ_n represent the input amplitude and phase of the *n*th element. $r_n \cdot \hat{r}$ is the position vector from the origin to the center of the *n*th element and the unit vector of the beam pointing direction.

The MMW slot antenna shows 45° polarization, and the elements are arranged horizontally along the *x*-axis instead of along their polarized direction, so that there is a superposition of gain both in the E- and H-plane with the equal amplitude in-phase feeding, which can also be seen in Fig. 9. In the process of antenna phased control, although the scanning angle is slightly weakened, two planes can be scanned at the same time. Fig. 10 shows the simulation and measurement results of the scanning performance of the millimeter wave band on the E-plane and H-plane. When the 3 dB scanning gain loss or -5 dB sidelobe level is met, the maximum scanning angle defined here can be achieved. The E-plane and H-plane simulations achieved a scanning angle of ± 30°. Due to the effect of port loss during the measurement, when the scanning angle of the E-plane beam reaches ± 25º, the beam coverage range is ± 35°, and when the scanning angle of the H-plane beam reaches ± 22 °, the beam coverage is ± 30°. As a result, MMW 1×4 arrays can support beam scanning angles of ± 22º on both the E- and H-planes.

Table 1 compares the proposed shared-aperture antenna with previously reported shared-aperture designs. The proposed design exhibits wider bandwidth and higher gain in both frequency bands, compared with [15], [16], [17]. Although the antenna arrays demonstrate high gain in [16] and [17], the antenna in [16] is powered by a single port leading to unattainable phased array, and the profile of the antenna in [17] is sacrificed for high gain. In contrast, this design utilizes separate feeding networks for each millimeter-wave array unit, enabling beam synthesis in both the E- and H-plane within the MMW band. Additionally, this work features a 45° polarization, which is the characteristic seldom discussed in the existing literatures.

IV. Conclusion

This paper has proposed a simple and low-cost MW and MMW shared-aperture antenna with wide bandwidths, high port isolations, flat in-band gains, and a low-profile characteristic. The antenna operates in the N78 and N257 frequency bands of 5G, with a measured 10 dB impedance bandwidth of 15.2% (3.26–3.81 GHz) and 12.8% (26.3–29.9 GHz), respectively. The in-band gains are approximately 8.8 dBi in the MW band and 11.9 dBi in the MMW band. The cross-polarizations are lower than -15dB in the MW band and -25 dB in the MMW band. In-band isolation is greater than 45 dB for both bands. The scanning capability study demonstrates that the MMW antenna array achieves ±22° beam scanning range in both the E- and H-plane.

References

[1] J. Gozalvez, "5G worldwide developments [mobile radio]," *IEEE Veh. Technol. Mag.*, vol. 12, no. 1, pp. 4-11, Mar. 2017.

[2] T. S. Rappaport, Y. Xing, "Overview of millimeter wave communications for Fifth-Generation (5G) wireless networks-with a focus on propagation models," *IEEE Trans. Antennas Propagat.*, vol. 65, no. 12, pp. 6213-6230, Dec. 2017.

[3] W. Hong, K.-H. Baek, and S. Ko, "Millimeter-wave 5G antennas for smartphones: overview and experimental demonstration," *IEEE Trans. Antennas Propagat.*, vol. 65, no. 12, pp. 6250-6261, Dec. 2017.

[4] W. Hong, "Solving the 5G mobile antenna puzzle: Assessing future directions for the 5G mobile antenna paradigm shift," *IEEE Microw. Mag.*, vol. 18, no. 7, pp. 86-102, Dec. 2017.

[5] H. -C, Huang, Huang, Huan-Chu. "Overview of 5G mm-wave antenna design solutions in cellular phones: AiP, AiA, and AiAiP," *IEEE International Symposium on Antennas and Propagat and USNC-URSI Radio Science Meeting*. IEEE, 2019.

[6] R. Rodriguez-Cano, S. Zhang, K. Zhao and G. F. Pedersen, "MM-wave beam-steerable endfire array embedded in a Slotted metal-frame LTE Antenna," *IEEE Trans. Antennas Propagat.*, vol. 68, no. 5, pp. 3685-3694, May. 2020.

[7] L. Zhang, K. Y. See, B. Zhang and Y. P. Zhang, "Integration of dual-band monopole and microstrip grid array for single-chip tri-band

application," *IEEE Trans. Antennas Propagat.*, vol. 61, no. 1, pp. 439-443, Jan. 2013.

[8] J. Zhang, K. Zhao, L. Wang, G. Pedersen, and S. Zhang, "Wideband low-profile dual-polarized phased array with endfire radiation patterns for 5G mobile applications," *IEEE Trans. Veh. Technol.*, vol. 70, no. 9, pp. 8431-8440, Sep. 202.

[9] K. Tekkouk, J. Hirokawa, R. Sauleau, M. Ettorre, M. Sano and M. Ando, "Dual-Layer ridged waveguide slot array fed by a butler matrix with sidelobe control in the 60-GHz band," *IEEE Trans. Antennas Propagat.*, vol. 63, no. 9, pp. 3857-3867, Sept. 2015.

[10] D. Wang and C. H. Chan, "Multiband antenna for WiFi and WiGig communications," *IEEE Antennas Wireless Propagat Letters*, vol. 15, pp. 309-312, 2016.

[11] Y. R. Ding and Y. J. Cheng, "Ku/Ka dual-band dual-polarized shared-aperture beam-scanning antenna array with high isolation," in *IEEE Trans. Antennas Propagat.*, vol. 67, no. 4, pp. 2413-2422, Apr. 2019.

[12] C. Han, J. Huang, and K. Chang, "A high efficiency offset-fed X/ka-dual-band reflect array using thin membranes," *IEEE Trans. Antennas Propagat*., vol. 53, no. 9, pp. 2792-2798, Sep. 2005.

[13] T. Li and Z. N. Chen, "Metasurface-based shared-aperture 5G S/K-band antenna using characteristic mode analysis," I*EEE Trans. Antennas Propagat.*, vol. 66, no. 12, pp. 6742-6750, Dec. 2018.

[14] X. -H. Ding, W. -W. Yang, H. Tang, L. Guo and J. -X. Chen, "A dual-band shared-aperture antenna for microwave and millimeter-wave applications in 5G wireless communication," *IEEE Trans. Antennas Propagat.*, vol. 70, no. 12, pp. 12299-12304, Dec. 2022.

[15] J. F. Zhang, Y. J. Cheng, Y. R. Ding and C. X. Bai, "A dual-band shared-aperture antenna with large frequency ratio, high aperture reuse efficiency, and high channel isolation," *IEEE Trans Antennas Propagat.*, vol. 67, no. 2, pp. 853-860, Feb. 2019.

[16] Z. -X. Xia, K. W. Leung, N. Yang and K. Lu, "Compact dual-frequency antenna array with large frequency ratio," *IEEE Trans. Antennas Propagat.*, vol. 69, no. 4, pp. 2031-2040, Apr. 2021.

[17] J. Zhang, S. Zhang and G. F. Pedersen, "Dual-band structure reused antenna based on quasi-elliptic bandpass frequency selective surface for 5G application," *IEEE Trans. on Antennas and Propagat.*, vol. 68, no. 11, pp. 7612-7617, Nov. 2020.

[18] Xu G, Peng H, "Dual-band differential shifted-feed microstrip grid array antenna with two parasitic patches," *IEEE Trans. Antennas Propag*., 2020, 68(3): 2434-2439, Mar. 2020.

[19] Y. Huo, X. Dong and W. Xu, "5G cellular user equipment: from theory to practical hardware design," *IEEE Access*, vol. 5, pp. 13992-14010, 2017.

[20] R. Garg, Microstrip Antenna Design Handbook, Boston, MA, USA: Artech House, 2001.

[21] A. A. Baba, R. M. Hashmi, K. P. Esselle, M. Attygalle and D. Borg, "A millimeter-wave antenna system for wideband 2-D beam steering," *IEEE Trans Antennas Propagat.*, vol. 68, no. 5, pp. 3453-3464, May. 2020.